UCSF
UC San Francisco Previously Published Works

Title

Diverse Strategies Engaged in Establishing Stereotypic Wiring Patterns among Neurons Sharing a Common Input at the Visual System's First Synapse

Permalink

https://escholarship.org/uc/item/0x63x4dr

Journal

Journal of Neuroscience, 32(30)

ISSN

0270-6474

Authors

Dunn, Felice A
Wong, Rachel OL

Publication Date

2012-07-25

DOI

10.1523/jneurosci.1581-12.2012

Peer reviewed

Development/Plasticity/Repair

Diverse Strategies Engaged in Establishing Stereotypic Wiring Patterns among Neurons Sharing a Common Input at the Visual System's First Synapse

Felice A. Dunn and Rachel O.L. Wong

Department of Biological Structure, University of Washington, Seattle, Washington 98195

Sensory circuits use common strategies, such as convergence and divergence, typically at different synapses, to pool or distribute inputs. Inputs from different presynaptic cell types converge onto a common postsynaptic cell, acting together to shape neuronal output (Klausberger and Somogyi, 2008). Also, individual presynaptic cells contact several postsynaptic cell types, generating divergence of signals. Attaining such complex wiring patterns relies on the orchestration of many events across development, including axonal and dendritic growth and synapse formation and elimination (reviewed by Waites et al., 2005; Sanes and Yamagata, 2009). Recent work has focused on how distinct presynaptic cell types form stereotypic connections with an individual postsynaptic cell (Morgan et al., 2011; Williams et al., 2011), but how a single presynaptic cell type diverges to form distinct wiring patterns with multiple postsynaptic cell types during development remains unexplored. Here we take advantage of the compactness of the visual system's first synapse to observe development of such a circuit in mouse retina. By imaging three types of postsynaptic bipolar cells and their common photoreceptor targets across development, we found that distinct bipolar cell types engage in disparate dendritic growth behaviors, exhibit targeted or exploratory approaches to contact photoreceptors, and adhere differently to the synaptotropic model of establishing synaptic territories. Furthermore each type establishes its final connectivity patterns with the same afferents on separate time scales. We propose that such differences in strategy and timeline could facilitate the division of common inputs among multiple postsynaptic cell types to create parallel circuits with diverse function.

Introduction

Located between cone photoreceptors and cone bipolar cells, the first synapse of the visual system is a critical locale for setting up spatial receptive fields, temporal filtering, and spectral discrimination (Dacey, 1996; Freed, 2000; Armstrong-Gold and Rieke, 2003). The first synapse also exhibits both divergence and convergence (Masland, 2001; Wässle, 2004). A single cone photoreceptor contacts each of the 8–11 types of cone bipolar cells (Wässle et al., 2009), so that each point in space is sampled by parallel pathways. Conversely, each type of bipolar cell receives input from a stereotyped number of photoreceptors (Wässle et al., 2009). Bipolar cells differentiate last of all retinal neurons (Cepko et

al., 1996). As such, cone photoreceptors and their unbranched axons have already established their laminar location in the outer retina even before bipolar cell dendrites elaborate (Morgan et al., 2006). Similarly, the apical dendrites of CA1 hippocampal neurons extend to contact already present glutamatergic afferents (Tyzio et al., 1999) and zebrafish retinal ganglion cell dendrites elaborate to reach stratified presynaptic amacrine cell processes (Mumm et al., 2006). But how multiple types of postsynaptic cells carve out their own patterns of connections in a stable field of afferents remains unclear. Timing and/or strategy could distinguish how dendrites of distinct cell types aiming for common afferents create unique connectivity patterns. For example, in competing for the same resources, dendrites that appear earlier and grow faster could win a greater number of synapses with afferents. Likewise dendritic growth strategies, such as stabilizing at synaptic sites (synaptotropic model; Vaughn et al., 1988; Niell et al., 2004, 2006), and variations on such rules could generate diversity of connectivity in a postsynaptic population.

To discriminate between these possibilities, we take advantage of the extensive classification of retinal neurons (Ghosh et al., 2004; Wässle et al., 2009) and short-range connections formed by three types of ON cone bipolar cells, with varying arbor sizes, and their cone targets. We chose to study types 6, 7, and 8 cone bipolar cells, which express the same glutamate receptors, contact cones nonselectively, and can be classified easily. Despite the similarities, we found differences across these bipolar cell types: dendritic territories remodel to different extents and dendrites establish synaptic contacts with different strategies; the magnitude of remodeling

correlated with arbor size. The small-field type 6 bipolar cells show a targeted approach, forming stable connections with cones and eliminating partners minimally, and thus adhering to the synaptotropic model (Vaughn et al., 1988; Niell et al., 2004, 2006). In contrast, large-field type 8 bipolar cells are more exploratory, forming transient connections with cones, eventually pruning a subset of contacts, and thus growing in a nonsynaptotropic manner. Also, each bipolar cell type attains a different final connectivity pattern with cones by a separate timeline—days versus weeks and before or after eye opening. Together our findings raise the possibility that the distinct strategies and timelines of developing postsynaptic cell types facilitate the unequal allocation of a common input to generate diverse parallel processing circuits.

Materials and Methods

Mice. The following transgenic mouse lines were used to visualize neurons in the retina: *hLM-GFP* (Fei and Hughes, 2001), which expressed GFP in cone photoreceptors containing middle-wavelength-sensitive (M) opsin; *Grm6-tdTomato*, which expressed TdTomato in a subset of ON bipolar cells under the metabotropic glutamate receptor 6 (mGluR6) promoter (Kerschensteiner et al., 2009); and *GUS8.4-GFP*, which expressed GFP in type 7 ON cone bipolar and rod bipolar cells under the gustducin promoter (Wong et al., 1999; Huang et al., 2003). Mice of either sex were used.

Tissue preparation. All procedures were performed in accordance with the University of Washington Institutional Animal Care and Use Committee protocols. Mice were killed with 5% isoflurane. Eyes were enucleated and immersed in oxygenated mouse artificial CSF (ACSF) containing the following (in mM): 119 NaCl, 2.5 KCl, 2.5 CaCl$_2$, 1.3 MgCl$_2$, 1 NaH$_2$PO$_4$, 11 glucose, and 20 HEPES. ACSF was brought to pH 7.42 with NaOH. For immunohistochemistry, retinas were isolated, mounted flat onto filter paper (Millipore) or left in the eyecup for sectioning, and fixed in 4% paraformaldehyde for 15–30 min, then rinsed in PBS, pH 7.42. Vibratome sections of 60–200 μm were made of isolated retinas mounted in agarose. Sliced or flat-mount retina were removed from the filter paper during immunoprocessing.

The following antibodies were used for immunolabeling: cone arrestin/Arr4 (1:500 and 1:1000; Zhu et al., 2002; Nikonov et al., 2008), peanut agglutinin-Alexa 647 (1:500; Invitrogen), synaptotagmin 2/znp-1 (1:1000; Zebrafish International Resource Center), and mGluR6 (1:100; Morgans et al., 2006). For secondary antibodies, Alexa-488, 568, 633 (1:1000; Invitrogen) or DyLight-488 (1:1000; Jackson Laboratory) conjugates were used.

To label cones, we started with the transgenic line *hLM-GFP*, in which cone photoreceptors with M-opsin express green fluorescent protein. Because the cone mosaic was incomplete, we additionally immunolabeled for cone arrestin, which accounted for most cones in the mouse retina, as evidenced by the uniform coverage of space (see Fig. 4a). At most, our labeling methods may have missed the 3% of cones containing pure short-wavelength-sensitive (S) opsin. However, additional labeling with peanut agglutinin (PNA), which should be found in all cones, did not further reveal any cones that were not already labeled by GFP or cone arrestin immunolabeling (data not shown). In some cones, labeling was weak but present nonetheless, and perhaps these cones contained S-opsin alone (see Fig. 4a, second row, central cone). We tried to include equally dim and bright cones in our analysis because all levels of fluorescence were converted into a binary mask (see Fig. 4d, second row). We relied on cone arrestin labeling for our study because we could not label cones with PNA at younger ages.

For live imaging, retinas were isolated, mounted flat onto filter paper (Millipore), and perfused with bicarbonate buffered Ames solution (Sigma) bubbled with 95% oxygen and 5% carbon dioxide. The recording chamber was kept at 30–33°C.

Imaging. Fixed tissue was imaged on a FV-1000 Olympus laser scanning microscope with an oil-immersion Olympus 60× objective (1.35 NA). Voxel sizes were between 0.05 and 0.14 μm/pixel (x-axis, y-axis) and 0.2–0.3 μm/pixel (z-axis). Live retina was imaged on a custom-built
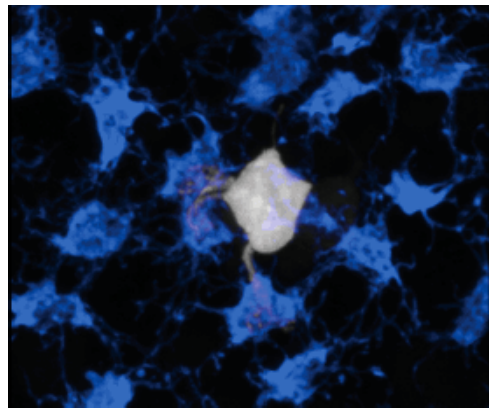
Movie 1. Synapse between cone photoreceptors and ON cone bipolar cell dendrites. Reconstruction of bipolar cell dendrites and cone terminals. Movie showing the synapses of cone photoreceptors (blue) and a type 6 ON cone bipolar cell (gray). As the image rotates, the bipolar cell dendrites are masked in yellow and the cones are masked in blue. The cone channel is flashed off to illustrate how the bipolar cell dendrites terminate within the cone terminals. Age, P30.

two-photon microscope with a Ti:sapphire laser (Spectra Physics) set to 890–930 nm with a water-immersion Olympus 60× objective (1.1 NA). Voxel sizes were 0.077 μm/pixel (x-axis, y-axis) and 0.5 μm/pixel (z-axis). Each plane was averaged 3–4 times (Kalman filter). With both methods of imaging, flat-mounted retinas were oriented with ganglion cell-side up, which produced less light scatter and clearer images than the opposite orientation.

Analysis. Images were processed with MetaMorph (Universal Imaging) and Amira (Mercury Computer Systems). All images were median filtered. Images used for figures were further processed in Photoshop (Adobe) by adjusting brightness and contrast, levels, and hues. For image analysis, we created a binary mask of bipolar cell dendrites, cone terminals, and mGluR6 labeling using a combination of a marching threshold and manual tracing plane by plane (Movie 1). By removing the soma from the mask, we focused our analysis on the dendrites. In some cells a dendrite located immediately above the soma looks like part of the soma in the two-dimensional projection; however, we could easily distinguish dendrites from the soma in the three-dimensional image. Two measures of the bipolar cell dendrites were taken: (1) bipolar cell dendritic territory, defined as the area within the convex polygon around the dendrites, and (2) bipolar cell dendritic area, taken as the total area of the two-dimensional maximum projection of the masks.

Each cone within the bipolar cell's dendritic field was labeled with a separate identity, enabling us to count unique cone contacts. These binary masks were imported into Matlab (Mathworks) for analysis (programs modified from code originally written by Josh Morgan). Statistics of the binary masks were either taken of the entire stack (volume) or of the two-dimensional projection (area) along the axis of the bipolar cell axon stalk. We measured the area and volume overlap between bipolar cell dendrites and cone terminals. The overlap areas and volumes were either averaged across all the cones contacted within the bipolar cell's dendritic field (see Fig. 5a,c) or were summed across all the cones within the bipolar cell's dendritic field (see Fig. 5b,d). A cone was considered to be contacted by the bipolar cell if there was nonzero area or volume overlap with bipolar cell dendrites. To obtain the average overlap per cone within the bipolar cell's dendritic field (see Fig. 5a,c), the total overlap per bipolar cell (see Fig. 5b,d) was divided by the number of cones contacted (see Fig. 5e).

Statistical analysis. In Figure 5e, a one-way ANOVA was used to test for differences in the number of cones contacted across ages at or after postnatal day 13 (≥P13). In Figure 7e, a paired *t* test was used to test for differences in the numbers of cones contacted as determined by two-way overlap between bipolar cell dendrites and cones or by three-way overlap among bipolar cell dendrites, cones, and mGluR6 labeling.
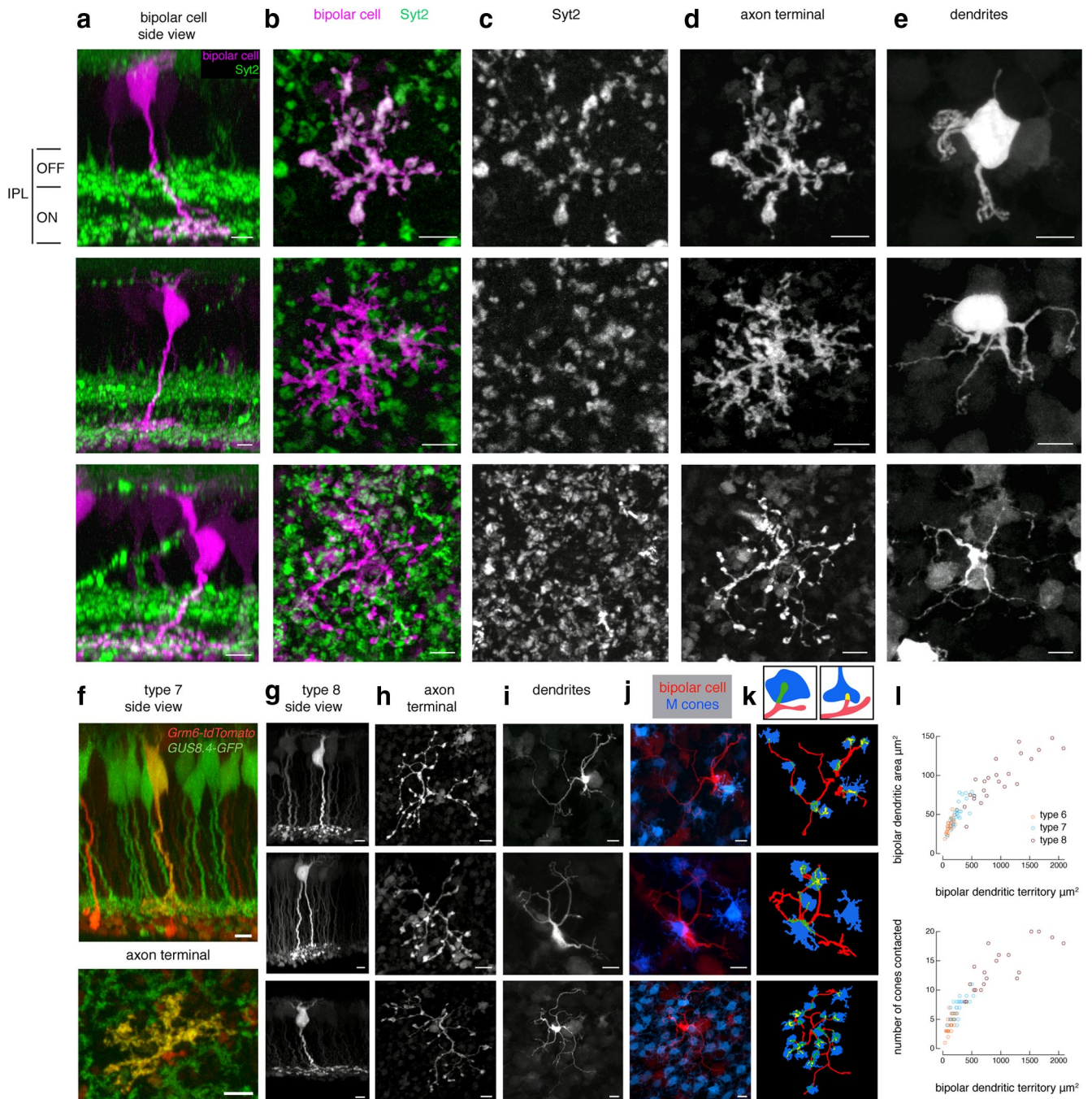
Figure 1. Bipolar cell types labeled in *Grm6-tdTomato* retina. Three types of ON cone bipolar cells in the *Grm6-tdTomato* transgenic mouse line. *a*, Side views of P30 retina with immunolabeling for Syt2 (green) show that the type 6 cone bipolar cell (magenta) stratifies vertically and broadly throughout the ON sublamina of the inner plexiform layer (IPL), type 7 stratifies at the top of the Syt2-positive band, and type 8 stratifies laterally and broadly throughout the lower part of the ON sublamina. *b*, En face views at the level of the axon terminals (magenta) with Syt2 (green) labeling. *c*, *d*, Type 6 axon terminals were the only ON bipolar cells with Syt2 labeling. Syt2 labeling alone (*c*). Bipolar cell axon terminals alone (*d*). *e*, Dendritic arbors of the bipolar cell types. *f*, Side view of a type 7 double labeled in the *Grm6-tdTomato* × *GUS8.4-GFP* line shows narrow stratification of the axon. En face view of the axon terminal shows overlap between tdTomato and GFP channels (yellow, bottom). Type 7 example from P30. *g*– *k*, Three examples of P59 large-field bipolar cells in the *hLM-GFP* × *Grm6-tdTomato* line. Side view of the entire bipolar cell (*g*). En face views of the axon terminal (*h*) and dendrites (*i*). Bipolar cell dendrites (red) and any cones expressing M opsin (blue) (*j*). Two-dimensional projections of binary masks with bipolar cell dendrites (red), M cones (blue), area overlap (green), and volume overlap (yellow) (*k*). Contacts between the dendrites of the large-field bipolar cells and cones expressing M-opsin suggest that these bipolar cells are type 8 rather than type 9, which are the other large-field bipolar cells that exclusively contact cones containing pure S-opsin (Haverkamp et al., 2005). The variability in the number of cone contacts shown here is because not all cones in the *hLM-GFP* line express GFP and because expression varies across the dorsal–ventral axis of the retina. *l*, Scatterplots of classified types 6, 7, and 8 bipolar cell dendritic territory and dendritic area, and of bipolar cell dendritic territory and number of cones contacted at P30 (see Materials and Methods for definition of parameters). Each point represents a single bipolar cell. Scale bars, 5 μm.

Results

Identifying cone bipolar cell types in the *Grm6-tdTomato* retina

In the *Grm6-tdTomato* transgenic line (Kerschensteiner et al., 2009), fluorescent protein is expressed by a subset of rod bipolar cells and ON cone bipolar cells. Expression was sufficiently sparse in some regions to allow single cells to be distinguished from their neighbors. Using a combination of morphological cues and cell-type-specific immunolabels to identify bipolar cell types according to the classification scheme of Wässle and colleagues (Wässle

et al., 2009), we identified three ON cone bipolar cell types in the *Grm6-tdTomato* line: types 6, 7, and 8 (Fig. 1). Two of these types, 6 and 8, have dendrites that have not been described previously in detail. The axon terminals of these bipolar cell types differed in their size and stratification levels within the inner plexiform layer (Fig. 1*a*,*d*). The axon of the type 6 immunolabeled for the calcium sensor, synaptotagmin 2 (Syt2; Fig. 1*b*,*c*; Fox and Sanes, 2007; Wässle et al., 2009), had bulbous terminals, and stratified broadly across sublaminae 3–5 of the inner plexiform layer (Fig. 1). The type 7 cone bipolar cell colabeled with *GUS8.3-GFP* (Wong et al., 1999; Huang et al., 2003), enabling us to determine that the type 7 had a scraggly looking axon terminal that stratified narrowly at the border between sublaminae 3 and 4 of the inner plexiform layer (Fig. 1*a*,*d*,*f*). The type 8 cone bipolar cell could be distinguished by its large axon terminal in sublaminae 4–5. Type 8 axons were sparse and had thin processes that connected varicosities (Fig. 1*d*,*g*,*h*).

The dendritic morphology of the bipolar cells also provided distinguishing features for classification (Fig. 1*e*). Type 6 bipolar cells had few branches (2–4 primary processes) and claw-like specializations at their dendritic terminals. The type 7 bipolar cells had more branches and smaller terminal specializations. The type 8 bipolar cells had the largest dendritic field and tended to have smoother dendritic terminals (Fig. 1*i*). Furthermore, these large-field bipolar cells contacted cones containing M-opsin, suggesting that these large-field bipolar cells are not type 9 cone bipolar cells, which exclusively contact cones with pure S-opsin (Haverkamp et al., 2005) (Fig. 1*j*,*k*). Scatterplots of bipolar cell dendritic parameters (e.g., area, territory, and number of cones contacted) show that the types 6 and 7 overlapped more than the type 8 (see Materials and Methods for explanation of parameters; Fig. 1*l*). However, the types 6 and 7 could be distinguished by additional criteria of Syt2 immunolabeling and axon stratification. Thus, we used a combination of axon stratification, dendritic field size and morphology, and immunolabeling to identify type 6, 7, and 8 cone bipolar cells.

Dendritic arbors across bipolar cell types simplify with maturation

We found that type 6, 7, and 8 bipolar cells could be reliably identified from P9 through adulthood. Figure 2 shows examples of each of the cell types at two time points during development: at P13, coincident with eye opening in the mouse, and at P30, when bipolar cells have adopted a stereotypic morphology. The dendritic trees of all three cell types simplified with age, losing branches over time (Fig. 2*a*–*c*), as shown previously for the type 7 cone bipolar cells (Lee et al., 2011). To quantify these changes, we created a binary mask of the dendrites by setting a marching threshold and tracing manually the dendrites of the cell within the three-dimensional image stack (see Materials and Methods). The two-dimensional projections of these masks were overlaid on the confocal images (Fig. 2*a*–*c*) and used to determine the convex polygonal area around the dendritic terminals (Fig. 2*d*). This dendritic territory corresponds to the region within which the cell can potentially contact its presynaptic partners, the photoreceptors. All three cell types showed a similar trend of territory expansion followed by different extents of reduction with maturation (Fig. 2*d*). At P30, type 6 bipolar cells had the smallest dendritic territory, followed by type 7 and type 8 cells (Fig. 2*d*). These cell-type differences in dendritic territories were established by the time of eye opening (P13). The total area of the two-dimensional mask projections, which we call dendritic area, is plotted in Figure 2*e*. The dendritic area approximates the total
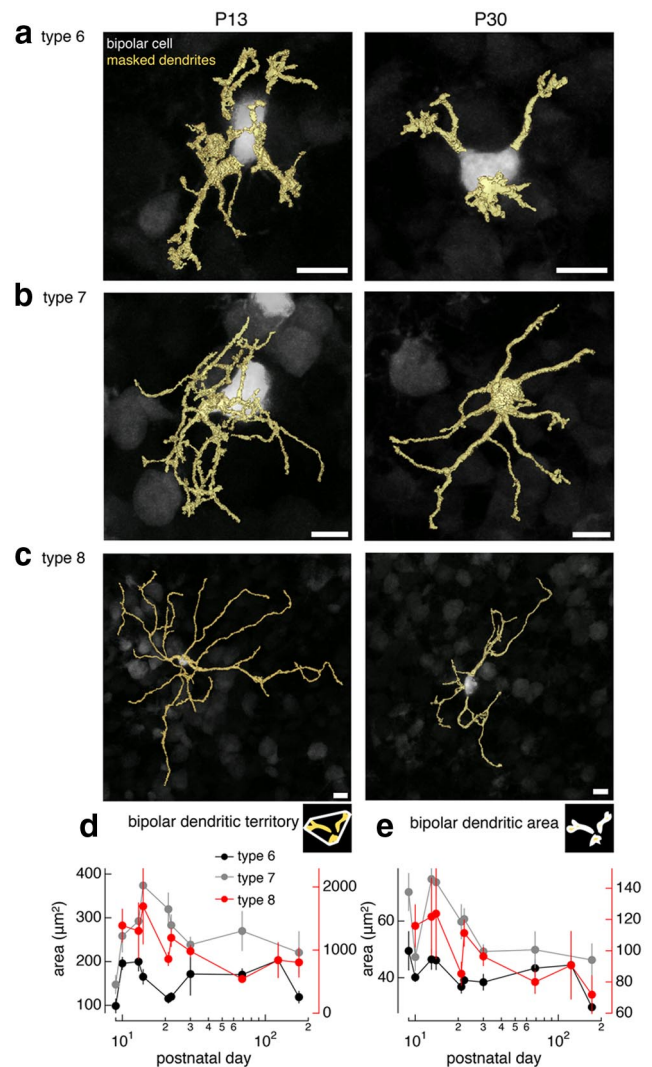

Figure 2. Developmental alterations in dendritic patterns vary with bipolar cell type. *a*–*c*, Examples of type 6 (*a*), 7 (*b*), 8 (*c*) ON cone bipolar cell dendrites at P13 (left column) and at P30 (right column) with binary masks of dendrites overlaid in yellow. *d*, Bipolar cell dendritic territory as a function of age. In the diagram, white lines around yellow bipolar cell dendrites represent measure taken. *e*, Bipolar cell dendritic area at different ages. For *d* and *e*, ordinate axis (μm^2) for types 6 and 7 on the left and for type 8 on the right. Points represent mean ± SEM. Number of cells listed in Table 1. Scale bars: *a*–*c*, 5 μm.

length and width of dendrites. The dendritic areas of type 6, 7, and 8 bipolar cells decreased between P9 and P30. Thus, on average, dendritic territories and areas underwent growth and remodeling during a developmental time period 5 d before and 2 weeks after eye opening (Table 1). These changes are consistent with the observations that dendritic trees simplify with age and that bipolar cell morphology is stereotyped by P30.

Bipolar cell types demonstrate distinct dendritic behaviors and territorial changes

At the earliest time point imaged, P9, the differences in dendritic territories of type 6, 7, and 8 bipolar cells suggest that either large-field type 8 bipolar cells initiate growth earlier and/or grow at faster rates. To determine whether dendritic growth rates differ across bipolar cell types, we imaged individual cells in live retina over the course of a day using two-photon microscopy. We focused on P12, the earliest age when isolated bipolar cells are labeled sufficiently brightly in the *Grm6-tdTomato* mouse, and the

Table 1. Summary of cone bipolar cell and cone photoreceptor measurements

Cone bipolar type and age	n	Bipolar area (μm^2)	Bipolar territory area (μm^2)	Bipolar volume (μm^3)	Area overlap per cone (μm^2)	Volume overlap per cone (μm^3)	Area overlap per bipolar cell (μm^2)	Volume overlap per bipolar cell (μm^3)	Number of cones contacted (volume criterion)	Number of cones contacted (area criterion)	Cone area (μm^2)	Cone density (cones/mm^2)
Type 6												
P9 (slice)	12	49.5 ± 6.9	98.7 ± 16.8	45.1 ± 9.7	6.8 ± 1.1	0.2 ± 0.7	24.8 ± 5.1	0.5 ± 0.2	1.8 ± 0.4	3.5 ± 0.5	14.5 ± 1.4	NA
P10	13	40.1 ± 1.6	195.6 ± 14.8	35.4 ± 3.1	4.9 ± 0.4	1.8 ± 0.3	25.0 ± 1.9	6.9 ± 1.2	4.2 ± 0.4	5.3 ± 0.4	18.2 ± 1.5	16,722 ± 970
P13	18	46.5 ± 3.6	199.8 ± 22.2	39.1 ± 3.4	5.5 ± 0.5	1.8 ± 0.3	29.6 ± 2.7	7.9 ± 1.4	4.7 ± 0.5	5.7 ± 0.4	16.7 ± 0.9	16,851 ± 801
P14	9	46.1 ± 3.4	165.2 ± 17.4	45.9 ± 3.6	5.5 ± 0.5	1.8 ± 0.2	31.8 ± 1.6	7.5 ± 0.9	4.3 ± 0.3	6.0 ± 0.3	18.9 ± 1.5	16,160 ± 868
P21	12	36.8 ± 2.4	115.2 ± 11.2	50.6 ± 6.2	8.1 ± 0.9	4.1 ± 0.7	34.1 ± 2.3	15.0 ± 2.4	4.1 ± 0.4	4.8 ± 0.5	26.0 ± 2.2	17,761 ± 1541
P22	19	39.1 ± 2.4	119.7 ± 10.1	64.4 ± 6.7	8.6 ± 0.7	2.4 ± 0.5	30.0 ± 1.7	7.7 ± 1.1	3.6 ± 0.3	3.8 ± 0.3	23.6 ± 1.5	15,405 ± 936
P30	27	38.4 ± 2.9	171.5 ± 49.2	46.3 ± 4.1	8.9 ± 0.6	4.8 ± 0.5	37.1 ± 2.8	17.6 ± 1.2	4.4 ± 0.4	4.7 ± 0.6	32.0 ± 1.3	14,852 ± 633
P69	20	43.4 ± 3.0	170.0 ± 14.3	51.3 ± 7.3	9.0 ± 0.3	4.1 ± 0.4	39.2 ± 1.8	17.3 ± 2.1	4.2 ± 0.2	4.4 ± 0.2	37.0 ± 1.4	12,512 ± 1003
P123	12	44.5 ± 4.1	203 ± 38.8	71.2 ± 10.4	10.3 ± 0.8	3.3 ± 0.8	31.1 ± 3.0	9.8 ± 2.1	3.2 ± 0.4	3.3 ± 0.4	33.0 ± 2.6	7344 ± 655
P172	11	29.6 ± 2.1	118.6 ± 14.4	28.8 ± 3.3	8.8 ± 1.0	3.6 ± 0.5	27.3 ± 2.4	11.4 ± 1.3	3.3 ± 0.2	3.3 ± 0.2	30.3 ± 2.6	11,678 ± 625
Type 7												
P9 (slice)	8	70.2 ± 6.7	147.4 ± 21.8	82.0 ± 28.3	6.6 ± 0.7	0.4 ± 0.1	33.3 ± 3.4	0.7 ± 0.3	2.9 ± 0.4	5.4 ± 0.7	14.6 ± 1.2	NA
P10	8	47.3 ± 4.9	258.4 ± 37.5	37.0 ± 3.8	3.6 ± 0.4	0.4 ± 0.1	23.0 ± 3.6	2.3 ± 0.5	5.3 ± 1.1	6.5 ± 1.1	14.8 ± 0.8	17,092 ± 1171
P13	19	74.8 ± 3.8	292.4 ± 21.7	60.0 ± 4.4	5.2 ± 0.3	1.1 ± 0.1	42.0 ± 3.5	7.8 ± 1.1	7.4 ± 0.7	8.3 ± 0.7	14.9 ± 0.6	15,883 ± 527
P14	9	73.7 ± 4.6	373.9 ± 39.2	72.3 ± 5.2	4.8 ± 0.2	0.9 ± 0.1	50.1 ± 3.8	7.3 ± 0.9	9.1 ± 1.2	10.6 ± 0.9	17.9 ± 0.5	17,037 ± 566
P21	12	59.8 ± 6.2	319.5 ± 37.9	58.4 ± 9.4	5.4 ± 0.4	1.2 ± 0.1	49.2 ± 5.5	10.4 ± 2.0	8.2 ± 0.7	9.2 ± 0.7	23.9 ± 1.8	18,303 ± 1102
P22	21	60.7 ± 3.8	282.9 ± 24.6	72.9 ± 5.5	6.5 ± 0.4	1.3 ± 0.3	47.4 ± 2.7	8.3 ± 1.5	6.6 ± 0.4	7.6 ± 0.5	23.5 ± 1.2	15,326 ± 636
P30	37	49.3 ± 2.5	238.5 ± 18.1	48.9 ± 3.5	6.9 ± 0.3	2.3 ± 0.2	46.0 ± 2.3	14.3 ± 1.2	6.5 ± 0.3	6.8 ± 0.3	31.6 ± 1.0	15,063 ± 448
P69	8	49.9 ± 6.5	269.8 ± 45.4	37.9 ± 4.6	6.0 ± 0.7	1.4 ± 0.3	35.4 ± 4.9	7.1 ± 0.6	5.4 ± 0.5	6.0 ± 0.5	30.0 ± 2.1	14,108 ± 1062
P172	3	46.3 ± 5.8	220.5 ± 48.6	37.0 ± 3.8	5.3 ± 0.4	1.4 ± 0.1	38.9 ± 6.4	9.1 ± 1.3	6.3 ± 0.3	7.3 ± 0.9	27.3 ± 2.1	15,065 ± 414
Type 8												
P10	10	115.9 ± 13.7	1389.7 ± 266.3	85.2 ± 8.9	3.1 ± 0.3	0.5 ± 0.1	54.5 ± 6.2	5.7 ± 0.8	13.1 ± 1.6	19.3 ± 3.2	16.7 ± 0.8	17,681 ± 2745
P13	8	121.7 ± 25.1	1303.6 ± 449.3	89.0 ± 17.5	3.2 ± 0.2	0.6 ± 0.1	61.9 ± 10.5	8.6 ± 1.5	14.8 ± 2.9	20.3 ± 4.3	16.2 ± 1.3	17,710 ± 1089
P14	7	123.7 ± 29.0	1692.3 ± 602.4	106.5 ± 24.2	3.8 ± 0.3	0.5 ± 0.1	81.3 ± 22.4	7.4 ± 2.0	17.1 ± 4.4	21.6 ± 5.2	19.9 ± 0.8	16,443 ± 662
P21	11	85.3 ± 7.6	859.6 ± 110.9	64.8 ± 4.0	4.3 ± 0.3	0.9 ± 0.1	74.9 ± 6.1	13.8 ± 1.8	15.5 ± 1.3	17.8 ± 1.6	23.5 ± 1.3	18,347 ± 1432
P22	14	111.3 ± 8.6	1194.5 ± 145.6	111.1 ± 9.4	5.0 ± 0.3	1.1 ± 0.2	87.9 ± 6.7	14.4 ± 2.4	14.1 ± 1.4	18.2 ± 1.6	24.7 ± 1.2	14,965 ± 530
P30	23	96.3 ± 6.1	983.7 ± 99.5	83.9 ± 5.9	5.8 ± 0.3	1.8 ± 0.1	93.1 ± 5.5	26.0 ± 2.1	14.7 ± 0.9	16.6 ± 1.0	31.1 ± 1.1	14,401 ± 505
P69	7	80.0 ± 7.6	541.9 ± 58.0	64.2 ± 6.9	6.4 ± 0.5	2.3 ± 0.3	70.8 ± 7.2	21.8 ± 1.7	10.1 ± 1.1	11.3 ± 1.2	30.7 ± 2.4	13,020 ± 1104
P123	3	90.7 ± 21.9	840.1 ± 283.3	109.4 ± 31.5	6.9 ± 0.5	3.2 ± 1.2	59.7 ± 2.2	22.3 ± 5.7	7.3 ± 0.7	8.7 ± 0.3	34.8 ± 8.7	7926 ± 2396
P172	6	71.8 ± 12.3	804.9 ± 239.3	56.6 ± 10.9	5.3 ± 0.7	1.7 ± 0.2	62.3 ± 10.4	16.0 ± 2.1	9.3 ± 0.7	11.7 ± 0.9	27.4 ± 2.9	13,368 ± 1824

Population data for all cone bipolar cells and cone photoreceptors. Data collected in flat mounts, otherwise noted (slice). Values reported are mean ± SEM. NA, not available.

onset of bipolar cell dendritic refinement. Indeed, at P12, dendrites of each bipolar cell type were motile, demonstrating extension and retraction of processes over 4–8 h intervals within a 24 h period of time-lapse imaging (Fig. 3a).

To quantify the observed dendritic changes for each cell, we plotted dendritic territory size (Fig. 3b) and dendritic area at each time point (Fig. 3d). We found that dendritic territories of type 6 and 7 bipolar cells increased or decreased <90 μm^2 per 4–8 h interval (Fig. 3c). In contrast, the territories of the type 8 cells changed as much as 400 μm^2 between time points (Fig. 3c), demonstrating large changes in spatial coverage of the dendritic arbor even within a day. However changes in the dendritic area were more similar across bipolar cell types, ranging from 0 to 40 μm^2 (Fig. 3e). These results suggest that extension and retraction of the dendrites of type 6, 7, and 8 bipolar cells occur at comparable rates. Dendritic changes of large-field type 8 bipolar cells appear dedicated to establishing or eliminating lateral territory, whereas dendritic changes of type 6 and 7 bipolar cells occurred largely within an established territory. Thus we find a simple relationship: the rate of dendritic territory remodeling correlates with the size of the dendritic arbor of type 6, 7, and 8 cone bipolar cells.

Bipolar cell types establish their mature cone contact patterns with different strategies

The differential magnitude of changes in dendritic territories of type 6, 7, and 8 bipolar cells raises the possibility that these bipolar cell types exhibit different ways of establishing their connections with cone photoreceptors. For instance, are the differences in the rates of establishing dendritic territory reflective of when the final number of cone contacts is established? Are changes in dendritic area important for establishing the amount of overlap between the bipolar cell dendrite and each cone? We explored these questions by determining the connectivity of each of the bipolar cell types with labeled cone photoreceptors at various ages. Each of these bipolar cell types contact multiple cone photoreceptor types: cones containing M-opsin, S-opsin, or both (Haverkamp et al., 2005). To visualize cones, we immunolabeled for cone arrestin (Zhu et al., 2002; Nikonov et al., 2008), a protein found generally in cone photoreceptors (Fig. 4a). S cones were labeled faintly yet could be distinguished adequately for our method of determining cone location (see Materials and Methods; also Haverkamp et al., 2005). We then quantified the patterns of connectivity across ages in three ways: (1) the amount of contact per cone, (2) the amount of contact per bipolar cell, and (3) the number of cones contacted by each bipolar cell.

En face views of the flat-mount retina show bipolar cell dendrites coursing underneath and terminating at cone pedicles (Fig. 4a,b). The innervation of ON bipolar cell dendrites into the cone terminals often occurs as an invaginating synapse (Movie 1), as shown previously by electron microscopy (Haverkamp et al., 2000). Thus, in the side view of the confocal stack, bipolar cell dendrites insert processes into the cone photoreceptor terminal (Fig. 4c). Quantification of overlap between the dendrites and
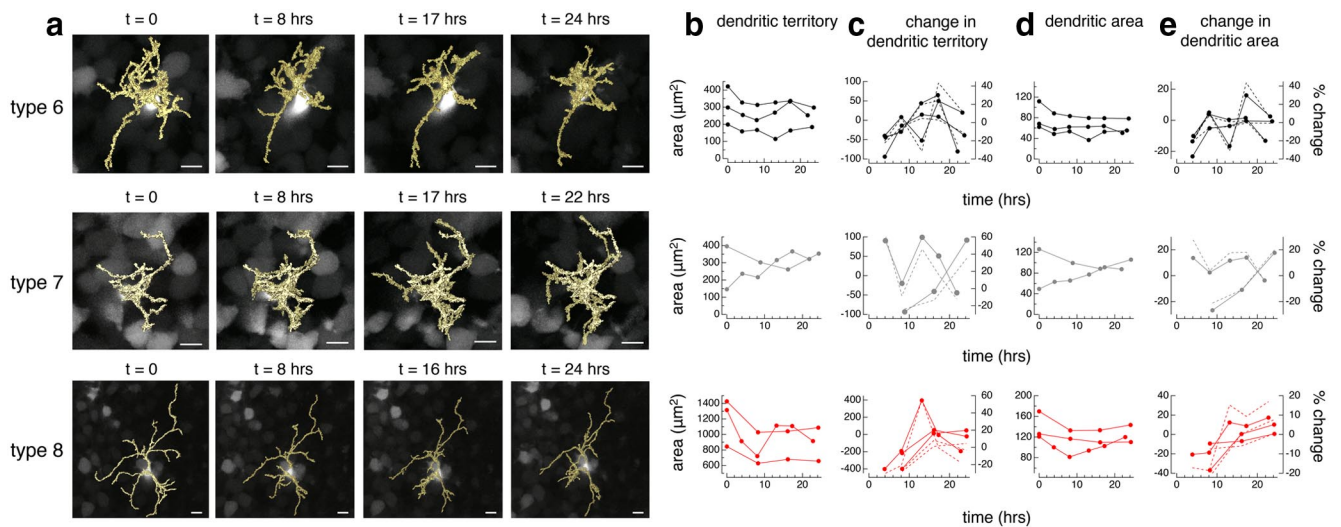
Figure 3. Bipolar cell types exhibit different dendritic growth behaviors. Two-photon time-lapse images of type 6, 7, and 8 ON cone bipolar cells in *Grm6-tdTomato* retina over a day. ***a***, Examples of bipolar cells at four time points with masked dendrites (yellow) overlaid on the raw images. ***b***, Bipolar cell dendritic territory for each cell at time points throughout a 24 h period. ***c***, Change in bipolar cell dendritic territory relative to the previous time point plotted as absolute area (left axis) and as percentage change in area (right axis). ***d***, Dendritic area at each time point. ***e***, Change in dendritic area relative to the previous time point plotted as absolute area (left axis) and as percentage change in area (right axis). Scale bars, 5 μm.

cone terminals relied on their respective binary masks (Fig. 4d,e). Area overlap is defined as where bipolar cell dendrites and cone terminals overlapped in the two-dimensional projections of the masks (Fig. 4d,e). These areas are considered sites of potential contact between presynaptic and postsynaptic cells, likely an overestimate of synapses actually made. A more stringent definition of contact is the volume of overlap between bipolar cell dendrites and cone terminals in three dimensions. These volumes comprise a subset of the space defined by the area overlap (Fig. 4d,e). Because of the resolution limits of light microscopy, particularly in the z-axis, we expect this volume overlap to be greater than that determined from electron microscopy.

For each bipolar cell, the average area or volume of overlap between each cone and the bipolar cell dendrites was plotted across age (Fig. 5a,c; Table 1). From the point of view of the cone, on average, each cone dedicated more territory and had greater contact with the small-field type 6 bipolar cells compared with the type 7 and 8 bipolar cells. This measurement averages across all cones contacted within the bipolar cell's dendritic field and ignores nonuniform overlap (Fig. 4d). When area overlap per bipolar cell was pooled over all the cones that the bipolar cell contacted, the smaller field type 6 and 7 bipolar cells on average had less overlap with cones than the type 8 cells (Fig. 5b). Thus, from the point of view of the bipolar cell, each type 6 and 7 bipolar cell showed less potential contact with cones than type 8, as reflected in their relative dendritic territory size (Fig. 2d). However, the actual amount of volume overlap between bipolar cell dendrites and cone terminals appears comparable among the three bipolar cell types up to P21. Beyond P21, type 8 bipolar cells possessed more total volume overlap with cones than the types 6 or 7 (Fig. 5d), suggesting that the type 8 bipolar cell may receive the greatest total synaptic input in the mature retina.

Each cone bipolar cell type we examined contacted a different total number of cones. In our analysis, a cone was considered to be contacted by the bipolar cell if there was any area overlap in the two-dimensional projection of the bipolar cell dendritic and cone masks or if there was volume overlap in the three-dimensional

masks (Fig. 5e). We considered the volume overlap criterion a conservative estimate of synaptic contacts compared with previously reported measurements using light microscopy of the type 7 cone bipolar cells (Wässle et al., 2009; Keeley and Reese, 2010). According to the volume overlap criterion, P30 type 6 cone bipolar cells contacted 4.4 ± 0.4 cones (mean $\pm$ SEM), type 7 contacted 6.5 ± 0.3 cones, and type 8 contacted 14.7 ± 0.9 cones (Table 1). Thus, if each bipolar cell type represents a parallel pathway in the retina, then the different number of convergent inputs at the first synapse in the retina may confer distinct bipolar cell response properties.

Furthermore, not only does each cone bipolar cell type receive input from a different number of cones, but each cone bipolar cell type achieved its mature connectivity by a different strategy: either by targeting or by exploring cones. With age, type 6 bipolar cells contacted an increasing number of cones until the mature number of contacts was attained (Fig. 5e). In contrast, type 7 and 8 bipolar cells contacted more cones early than in the mature retina; the number of cones contacted reached a peak at ~P13 and then declined with maturation (Fig. 5e). Thus, the strategies of type 7 and 8 bipolar cells for development involved a process of contacting more cones than are retained at maturity, whereas the type 6 bipolar cell only contacts up to the number of cones that are maintained at maturity. In summary, among the cone bipolar cell types we examined, type 6 bipolar cells contact the fewest cones and find those partners before the type 7 and 8 bipolar cells achieve their mature connectivity patterns.

Postsynaptic receptors are present at most dendritic invaginations into cone photoreceptors

To find out whether volume overlap between bipolar cell dendrites and cone photoreceptor terminals are indicative of synapses, we immunolabeled for the postsynaptic receptor, mGluR6, in addition to the cone photoreceptor and bipolar cell. Because mGluR6 is expressed on the dendrites of all ON cone bipolar and rod bipolar cells (Nomura et al., 1994; Vardi et al., 1998) (Fig. 6), we used the dendrites of individual bipolar cells as a mask to eliminate all mGluR6 signal outside the cell of interest (Fig. 7a–c). Distinguishing individual postsynaptic puncta requires higher resolution than is possible
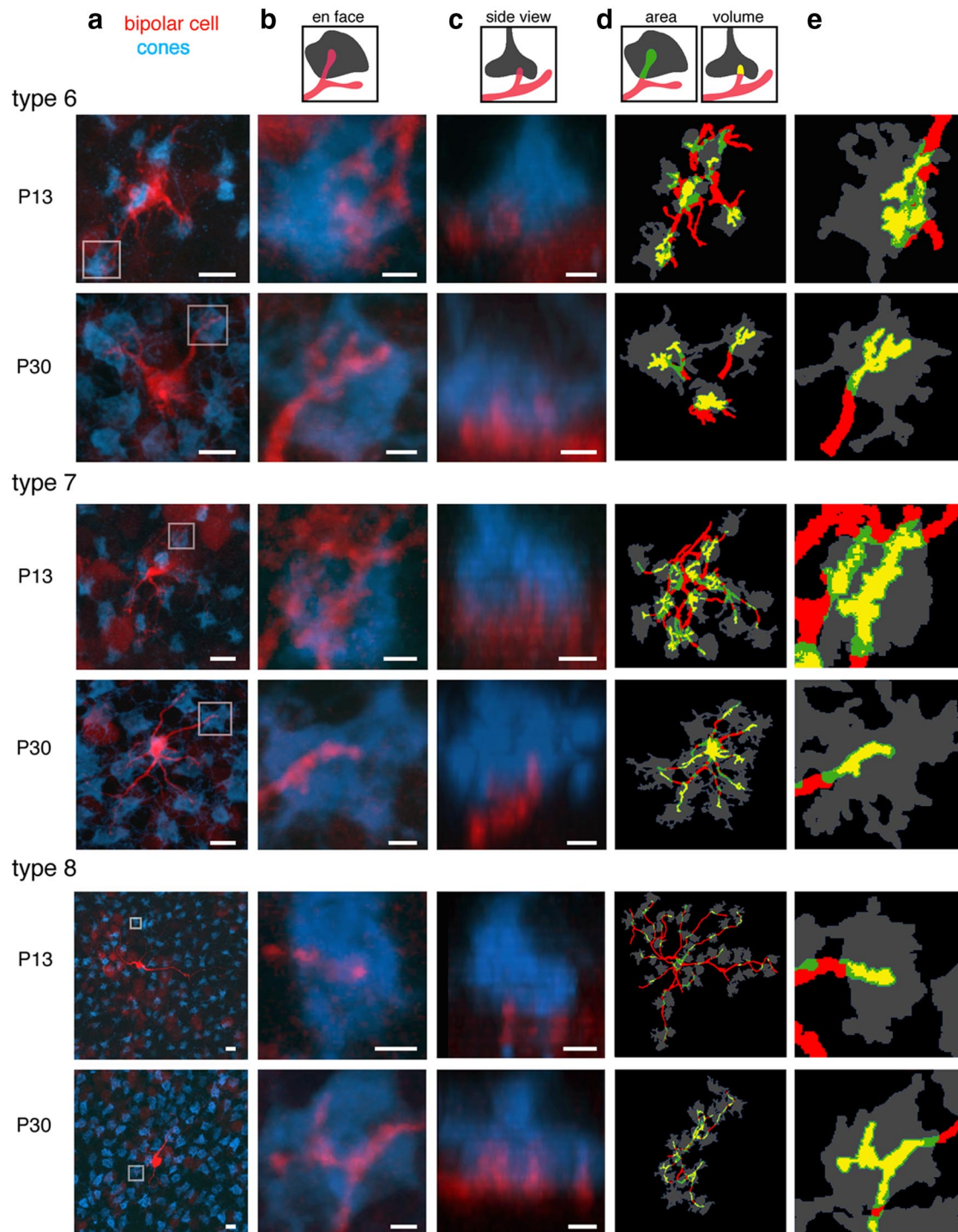
Figure 4. Visualization of contacts between cones and bipolar cell dendrites. Contacts between cone photoreceptor axons and bipolar cell dendrites at P13 (top row in each pair) and P30 (bottom row in each pair). ***a***, Confocal images of type 6, 7, and 8 ON cone bipolar cell dendrites (red) and cone arrestin labeling of cone terminals (blue). ***b***, ***c***, En face (***b***) and side (***c***) views of a single cone contacted by the bipolar cell dendrites, highlighted by the box in ***a***. ***d***, Two-dimensional projections of the binary masks with bipolar cell dendrites (red), cones (gray), area overlap (green), and volume overlap (yellow). ***e***, Magnified view of a single cone in the binary masks. Scale bars: ***a***, 5 μm; ***b***, ***c***, 1 μm.

with light microscopy. Thus we quantified the total volume overlap among the bipolar cell dendrites, cone photoreceptors, and postsynaptic receptors with the binary masks of all three channels rather than counting puncta.

We then compared two-way bipolar cell and cone volume overlap with the three-way bipolar cell, cone, and mGluR6 volume overlap (Fig. 7*d*). The linear dependence of these two measures across ages suggests that two-way volume overlap

predicts the presence of a postsynaptic receptor, and that the amount of mGluR6 present scales with the volume overlap between bipolar cell dendrites and cones. Thus, our measure of volume overlap between the bipolar cell dendrites and cone terminals provides a proportionally consistent estimate of a potential synapse.

The number of cones contacted was calculated for this dataset as in Figure 5*e*, where the criterion for a contact is either two-way vol-
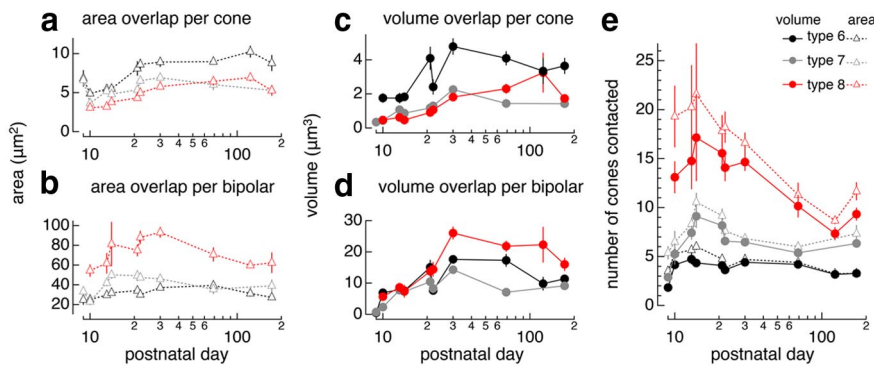
Figure 5. Bipolar cell types show distinct developmental changes in their contact with cones. Overlap between cone photoreceptors and bipolar cell dendrites quantified from binary masks. ***a***, ***b***, Summary of the average area overlap per cone within a bipolar cell's dendritic field (***a***) and for total area overlap with cones (***b***) for type 6 (black), type 7 (gray), and type 8 (red) cone bipolar cells. ***c***, ***d***, Summary of the average volume overlap per cone across ages (***c***) and for volume overlap per bipolar cell (***d***). ***e***, Summary of the number of cones each bipolar cell contacts as determined by the number of unique cones that overlap with bipolar cell dendrites in volume (closed circles) or area (open triangles). One-way ANOVA was used to test for differences in the number of cones contacted across ages $\geq$ P13. Type 6 volume $F_{(7,120)} = 1.8$, $p = 0.09$; type 6 area $F_{(7,120)} = 4.06$, $p = 0.0005$; type 7 volume $F_{(6,102)} = 3.13$, $p = 0.007$; type 7 area $F_{(6,102)} = 4.85$, $p = 0.0002$; type 8 volume $F_{(7,71)} = 2.07$, $p = 0.058$; type 8 area $F_{(7,71)} = 2.46$, $p = 0.026$. Points represent mean $\pm$ SEM. Number of cells listed in Table 1.
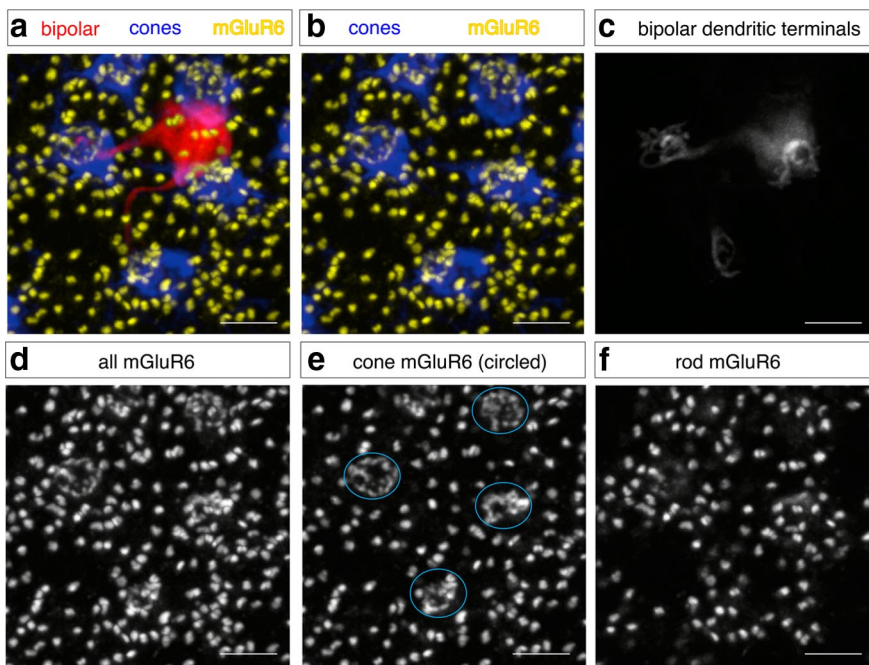

Figure 6. Distinction between postsynaptic receptors, mGluR6, within rod bipolar and ON cone bipolar cells. mGluR6 labeling in rod bipolar cells and ON cone bipolar cells has distinct morphologies and planar locations. ***a***, Confocal image of a type 6 cone bipolar cell (red), cone terminals (blue), and mGluR6 puncta (yellow). ***b***, mGluR6 (yellow) and cone arrestin immunolabeling (blue). ***c***, Bipolar cell dendritic terminals to illustrate where cones are contacted. ***d***, All mGluR6 alone. ***e***, Select planes of the mGluR6 to emphasize receptors found at the ON cone bipolar cell dendritic terminals, which tend to be clustered in ovals. Location of the cones are circled in blue. ***f***, Select planes of the mGluR6 to emphasize receptors found at rod bipolar cell dendritic terminals, which tend to be in pairs and punctate. Age, P172. Scale bars, 5 μm.

ume overlap between cones and bipolar cell dendrites, or three-way volume overlap with the presence of the postsynaptic receptor (Fig. 7e). The numbers of cones contacted by the type 6, 7, and 8 bipolar cells were not significantly different for both methods of counting contacts (paired *t* test, $p > 0.05$). This suggests that, when using volume overlap between bipolar cell dendrites and cones to count cone contacts, the results can be considered equivalent with or without postsynaptic receptors.

Stability of cone contacts during circuit development varies across bipolar cell types

Although the static views across ages revealed differences in the overall strategy by which type 6, 7, and 8 bipolar cells establish their final contact number, such views cannot reveal the stability or transience of the early contacts. Does a type 6 cone bipolar cell maintain contact with the same cones once the mature number is reached? Does a type 8 cone bipolar cell constantly exchange cones or establish a peak number of contacts before executing a phase of pruning? To answer these questions, we imaged in live retina individual bipolar cells and cones labeled in the *Grm6-tdTomato × hLM-GFP* transgenic line, where a subset of bipolar cells and cones express fluorescent protein (Fig. 8a,b). Between P14 and P15, we tracked bipolar cell dendritic contacts with individual cones for 16–24 h (Fig. 8c–f) and found dynamic area and volume overlap (Fig. 8g). A count of the number of cones contacted by each bipolar cell at each time point (Fig. 8h, each bipolar cell represented by a horizontal line) revealed that type 6 cone bipolar cells tended to maintain the same number and identity of cones contacted (0.13 $\pm$ 0.46 change in the absolute number of cones between time points for $n = 7$ cells, mean $\pm$ SD; range, 0–2 cones). In contrast, type 8 cone bipolar cells added and eliminated cone contacts over 4–8 h intervals (1.41 $\pm$ 1.94 change in the absolute number of cones between time points for $n = 6$ cells; range, 0–5 cones). Type 7 cone bipolar cells showed an intermediate behavior (0.87 $\pm$ 1.5 change in the absolute number of cones between time points for $n = 5$ cells; range, 0–4 cones). Thus if the observed behavior extends to a longer term, the live-imaging results suggest that type 6 bipolar cells maintain contact with the same subset of cones and that cones may stabilize their dendrites, whereas type 7 and 8 cells exchange cones during development and cone contacts alone fail to stabilize their dendrites.

Discussion
Different timelines and dendritic behaviors in establishing distinct cone-to-cone bipolar cell circuitry
In the nervous system, the onus of targeting appropriate synaptic partners can fall on axons (Huberman et al., 2008; Hashimoto et al., 2009; Leamey et al., 2009) or dendrites (Jefferis et al., 2004; Mumm et al., 2006). However, when we consider how neural circuits establish convergence and divergence, in addition to selecting right partner types, understanding circuit assembly becomes more challenging. Studies showing differences in dendritic growth behaviors examined neurons that receive input from different presynaptic partners
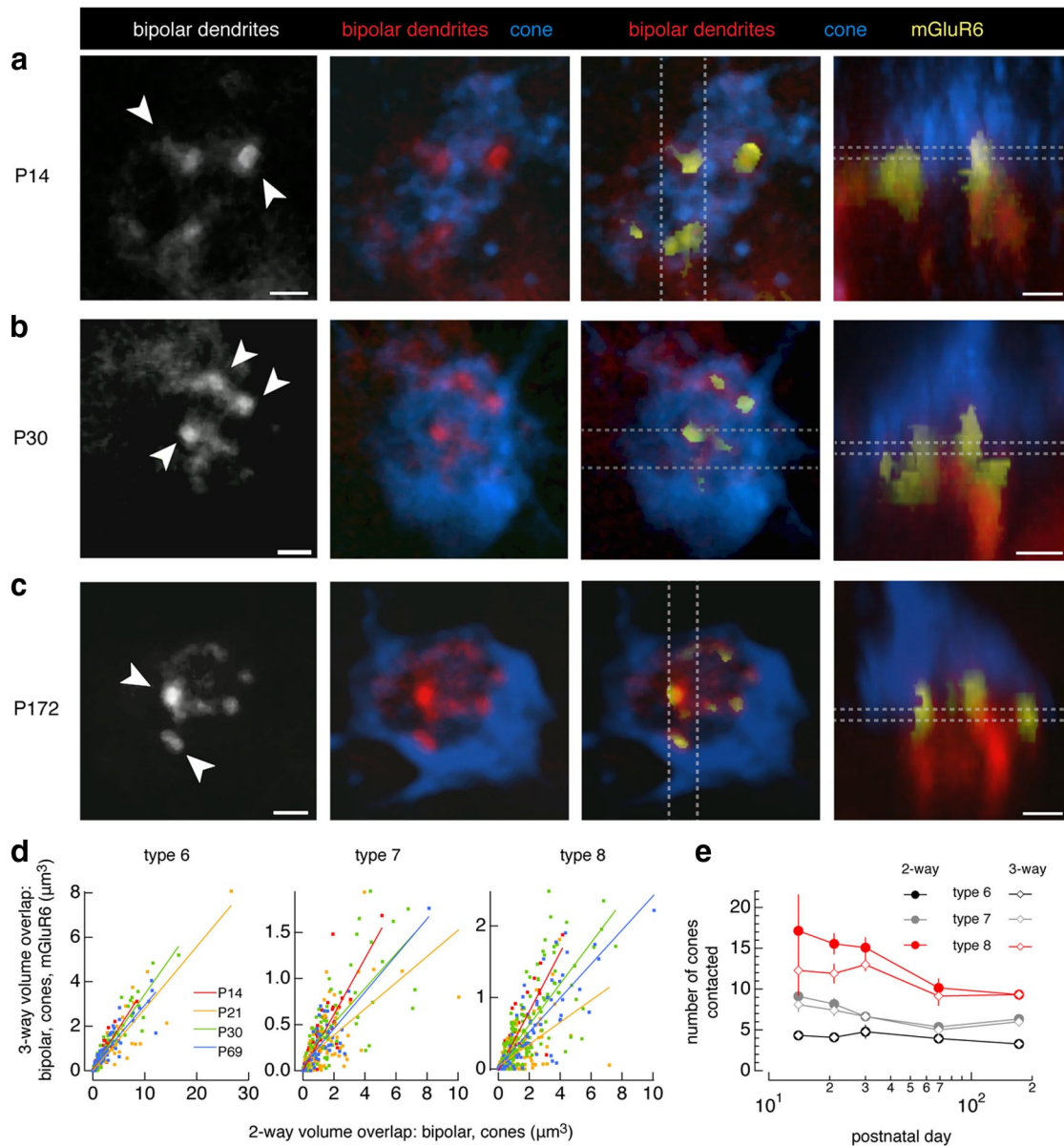
Figure 7. Postsynaptic receptors present at most dendritic invaginations into cone photoreceptors. Amount of postsynaptic receptors scales with overlap between bipolar cell dendrites and cones. ***a–c***, Examples of type 6 cone bipolar cell dendrites at P14 (***a***), P30 (***b***), and P172 (***c***). Single image plane of type 6 bipolar cell dendrites alone (first column). Single image plane of bipolar cell dendrites (red) and a cone (blue) (second column) and with mGluR6 (yellow) within bipolar cell dendritic masks (third column). Location of the single plane is indicated by the dotted lines in the fourth column. Side view of a stack of planes located between the dotted lines in the third column (fourth column). In the single plane view, the bipolar cell dendrites invaginate the cone at punctate locations, indicated by the white arrowheads. These punctate dendritic endings coincide with mGluR6 labeling. ***d***, Summary of volume overlap among bipolar cell dendrites, cones, and mGluR6 (three-way overlap) against volume overlap between bipolar cell dendrites and cones (two-way overlap) for different ages. Data points fit with line. ***e***, Number of cones contacted using volume overlap between bipolar cell and cones (2-way; closed circles) and among bipolar cell, cones, and mGluR6 (3-way; open diamonds) for the same dataset. A paired *t* test was used to compare the number of cones contacted at each age for two-way and three-way volume overlap criteria. The null hypothesis could not be rejected for all comparisons. Type 6 $p > 0.47$ [$n = 9$ (P14), 21 (P21), 13 (P30), 14 (P69), 12 (P123), 11 (P172)], type 7 $p > 0.46$ [$n = 9$ (P14), 12 (P21), 11 (P30), 8 (P69), 3 (P172)], type 8 $p > 0.05$ [$n = 7$ (P14), 11 (P21), 11 (P30), 7 (P69), 6 (P172)]. Scale bar, 1 μm.

(Mumm et al., 2006). Here, the cone-to-cone bipolar cell synapse provides a unique opportunity to contrast the development of different types of postsynaptic neurons contacting a single population of presynaptic cells. While cone densities and axonal areas continue to change over this developmental period (Table 1), the photoreceptor axons have laminated by P5 (Morgan et al., 2006). We were therefore able to unravel the strategies used by distinct postsynaptic partners contacting a layer of axonal terminals whose locations are determined even before dendritic outgrowth from postsynaptic cells begins (Morgan et al., 2006).

We found that type 6, 7, and 8 bipolar cells undergo changes in dendritic morphology and territory size that coincide with contacting cones and establishing postsynaptic sites. If we assume that bipolar cells contact every cone within its territory and that cone densities decrease from 17,000 to 14,000 cones/mm^2 (Table 1), then the changes in bipolar cell dendritic territory between P13 and P14 and >P69 predict that type 6's prune contacts by an average of 1.0 cone, type 7's prune 1.2 cones, and type 8's prune 14.5 cones. Indeed, our measurements demonstrated that these bipolar cell types prune to different extents: on average type 6 prunes 0.3–1.5 cones, type 7 prunes 1–2 cones, and type 8 prunes
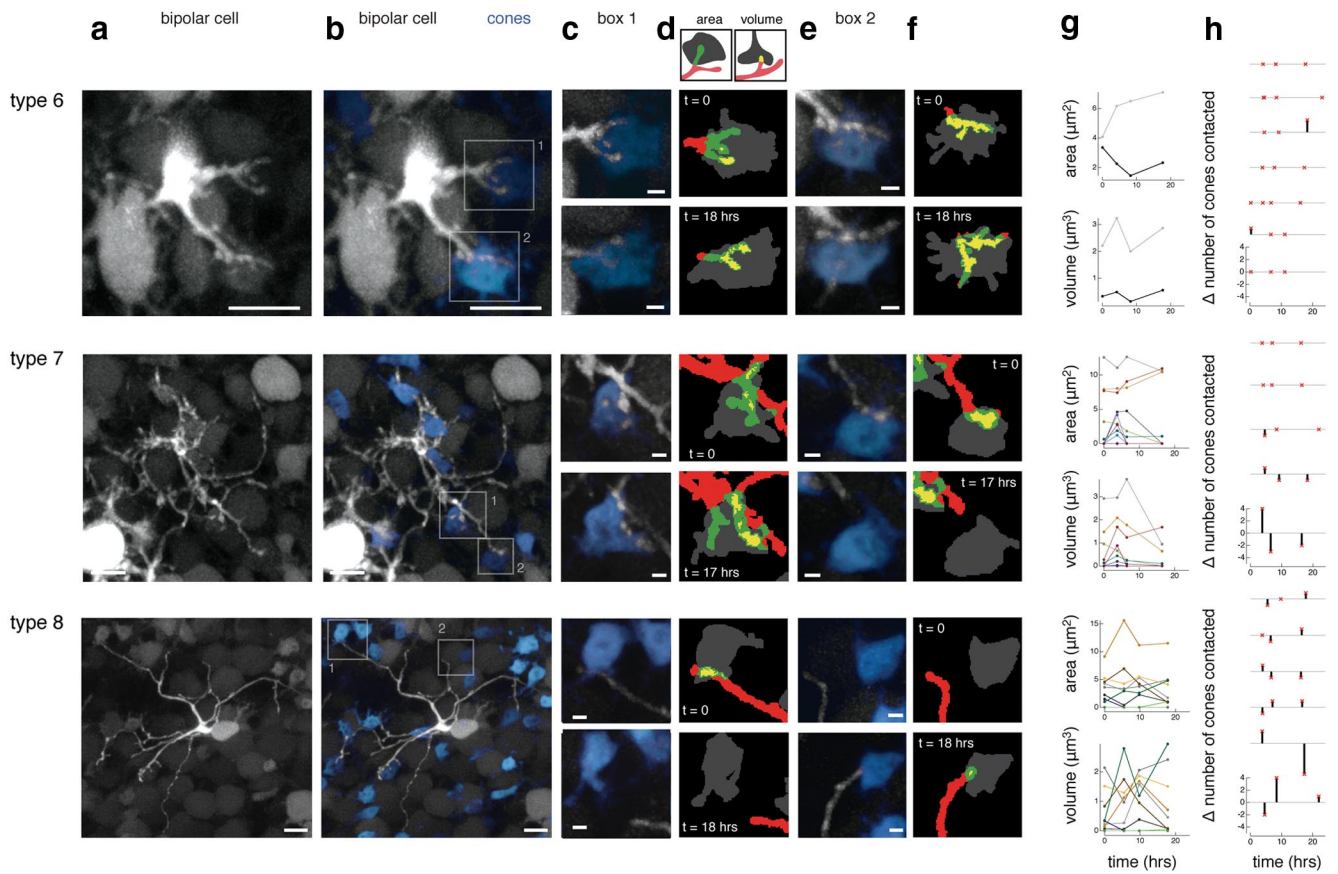
Figure 8. Large-field type 8 bipolar cells make more transient contacts with cones. Two-photon images of type 6, 7, and 8 ON cone bipolar cells and a subset of cones in the *Grm6-tdTomato* × *hLMcone-GFP* retina over the course of a day at P14–P15. ***a***, ***b***, Images of bipolar cells (***a***, gray) with cones (***b***, blue) at the first time point. ***c***, ***e***, Magnified view of the first and last time points, highlighted by the boxes in ***b***. ***d***, ***f***, Masked images of bipolar cell dendrites (red), cone (gray), area overlap (green), and volume overlap (yellow) at the first (top) and last (bottom) time points for two example cones. ***g***, Area (top) and volume (bottom) overlap between each cone within the bipolar cell's dendritic field shown in ***b***. Each line represents a different cone. ***h***, Change in the number of cones contacted by each bipolar cell imaged over the course of the time lapse using nonzero volume overlap as the criterion for contact. Each horizontal line represents a constant number of cones contacted between time points for an individual bipolar cell; ordinate axis applies to all cells. The red "x" marks the change in the number of cones at each time point and a vertical bar was drawn to the "x" for nonzero changes in cones contacted. Scale bars: ***a***, ***b***, 5 μm; ***c–f***, 1 μm.

7–9 cones. Thus, cone density and bipolar cell dendritic territory changes predict the targeted (type 6) versus exploratory strategies (types 7 and 8) of these cone bipolar cells in establishing connectivity with cones.

Our observations also show that despite sharing the same population of inputs, postsynaptic cells need not reach their individual and disparate connectivity patterns at the same time. In fact, the type 8 cone bipolar cells continued to change their number of cones contacted beyond P30, which was surprising considering the accepted notion of adult mouse retina at this age and how structural connectivity alters beyond eye opening. In the mouse olfactory system, developing olfactory receptor neurons expressing different receptors refine axons from spurious glomerular sites at different speeds, thus asynchronously reaching a mature morphology (Zou et al., 2004). Our study further demonstrates that dendrites of different postsynaptic cell types can likewise select final presynaptic partners on disparate timelines. Although different retinal ganglion cell types establish dendritic patterns with varying strategies (Mumm et al., 2006; Kim et al., 2010; Ren et al., 2010), such differences may be attributable to a unique complement of presynaptic amacrine and bipolar cells for each ganglion cell type. Conversely, our current findings emphasize that distinct strategies are used for establishing specific connectivity patterns between a single presynaptic cell population

and several morphologically separate and, probably, functionally distinct postsynaptic partners.

Disparate cone-to-cone bipolar cell connectivity patterns and functional predictions

Assuming equivalent inputs from each cone and other interneurons to bipolar cells and similar intrinsic properties of bipolar cells, differences in convergence predict that the small-field type 6 bipolar cell has a lower signal-to-noise ratio but is capable of encoding higher spatial resolution because, compared to other bipolar cells, type 6 bipolar cells have fewer cones to average over and presumably a smaller receptive field. In comparison, one might predict that the type 8 bipolar cell has a higher signal-to-noise ratio because of averaging across a greater number of cones but poor spatial resolution because its receptive field would be large. Convergence alone implies that response properties of bipolar cells are differentially tuned, setting up parallel pathways. However, as shown previously (Wässle et al., 2009) and presently, the amount of overlap between cones and bipolar cell dendrites differs by the bipolar cell type and by each individual contact, possibly implicating different synaptic strengths. In primate retina, electron micrographs reveal that not all ON cone bipolar cells make invaginating contacts with cones (Calkins et al., 1996; Hopkins and Boycott, 1996). Likewise, in the ground squirrel, OFF

cone bipolar cells make varied contacts with cones (DeVries et al., 2006). For the moment, let us assume that the amount of volume overlap we measured corresponds to synaptic strength. In support of this assumption, labeling for the postsynaptic glutamate receptor, mGluR6, suggests that the volume of bipolar cell dendritic overlap with cones correlates with the amount of mGluR6. For the small type 6 bipolar cell, greater overlap per cone (i.e., synaptic strength) compensates for fewer cone inputs. By the same argument, the large type 8 bipolar cell has more cone inputs but a smaller amount of overlap with each cone. Thus, convergence alone may be inadequate to predict the response properties of a bipolar cell. Our data point to a potential tradeoff between the number of convergent inputs and the strength of each input—a relationship established during development.

Potential mechanisms regulating connectivity patterns of bipolar cell types

In vivo observations of tectal neuron dendritic growth in zebrafish demonstrated that dendritic filopodia that encounter a correct presynaptic partner stabilize into a dendritic branch, while filopodia that fail to meet an appropriate partner retract (Niell et al., 2004; Chen et al., 2010). Such a synaptotropic method of dendritic growth maximizes the efficiency of finding local synaptic partners by selectively stabilizing dendrites in a region where desired afferents are present (Niell, 2006). According to this scheme, type 6 bipolar cells may grow synaptotropically as their dendrites find the nearest cones and establish synaptic contacts, consistent with stable dendritic connections with cones as viewed by time-lapse imaging. In contrast, the type 8 bipolar cell's long dendritic lengths without cone contacts and seemingly random cone choices together suggest that the dendritic patterning of this cell type cannot be described by the synaptotropic model (Niell, 2006), consistent with the more transient dendritic and cone connections. For the three cone bipolar cells investigated, we found that how dendrites grow with respect to their presynaptic partners correlated with cell size. Whether the correlation between cell size and growth behavior applies to other types of ON and OFF cone bipolar cells remains to be determined.

The cone-to-cone bipolar cell synapse is one of the many circuits in the nervous system where divergence and convergence necessarily involve dividing resources among multiple synaptic partners. While all bipolar cell types must share space on the cone, differences in size, tiling density, and dendritic morphology together suggest that each bipolar cell circuit could be established by distinct developmental programs and/or interactions between bipolar cells. Indeed, homotypic interactions that shape neuronal morphologies in the *Drosophila* visual (Millard et al., 2007) and olfactory (Zhu and Luo, 2004) systems have also been proposed to regulate dendritic territories and connectivity in the mammalian retina (Reese, 2005; Poché et al., 2008; Lee et al., 2011). Every reported retinal neuron type, including the type 6 and 7 cone bipolar cells, tile the retina in a regular array (Wässle et al., 2009), and we assume the same applies for the type 8 bipolar cell, whose mosaic remains unknown. If homotypic interactions influence dendritic growth and cone contacts, the dense dendritic morphology and high density of type 6 bipolar cells predict a high probability of interacting with a neighbor, thus capping further lateral growth, preventing extraneous cone contacts, and allowing for growth dedicated to making invaginations into cones. In contrast, the sparse dendritic branching and presumably low density of type 8 bipolar cells predict a lower probability of encountering a neighbor before extraneous dendritic branches and cone contacts are formed, thus requiring elimination of branches and cone contacts. Recent work has demonstrated that manipu-

lating the entire population of bipolar cells affects the dendritic field size of the type 7 cone bipolar cell (Lee et al., 2011), but the role of homotypic interactions remains to be determined by type-specific manipulations, which are not yet possible. Synaptotropic and nonsynaptotropic methods of establishing synaptic contacts could involve homotypic or heterotypic mechanisms of setting territory boundaries.

The greater dendritic invaginations of the type 6's over the type 8's could also result from intrinsic differences in the desired connectivity patterns and/or from heterotypic competition. For example, the type 8 may obtain less cone territory because of its later timing relative to the type 6. Alternatively, perhaps differences in the number and degree of contacts with cones relieve competition for overlapping resources (e.g., the type 6 aims for greater invaginations while type 8 aims for a greater number of cones), as implied by the differences in rates of territorial remodeling observed during live imaging. Whether distinct bipolar cell morphologies and connectivity patterns are preprogrammed or result from competition (e.g., homotypic or heterotypic), the development of the cone-to-cone bipolar cell synapse demonstrates that multiple postsynaptic neuronal types establish contacts with a single population of presynaptic partners with varying timelines and strategies.

References

Armstrong-Gold CE, Rieke F (2003) Bandpass filtering at the rod to second-order cell synapse in salamander (*Ambystoma tigrinum*) retina. J Neurosci 23:3796 –3806.

Calkins DJ, Tsukamoto Y, Sterling P (1996) Foveal cones form basal as well as invaginating junctions with diffuse ON bipolar cells. Vision Res 36:3373–3381.

Cepko CL, Austin CP, Yang X, Alexiades M, Ezzeddine D (1996) Cell fate determination in the vertebrate retina. Proc Natl Acad Sci 93:589–595.

Chen SX, Tari PK, She K, Haas K (2010) Neurexin-neuroligin cell adhesion complexes contribute to synaptotropic dendritogenesis via growth stabilization mechanisms in vivo. Neuron 67:967–983.

Dacey DM (1996) Circuitry for color coding in the primate retina. Proc Natl Acad Sci 93:582–588.

DeVries SH, Li W, Saszik S (2006) Parallel processing in two transmitter microenvironments at the cone photoreceptor synapse. Neuron 50:735–748.

Fei Y, Hughes TE (2001) Transgenic expression of the jellyfish green fluorescent protein in the cone photoreceptors of the mouse. Vis Neurosci 18:615–623.

Fox MA, Sanes JR (2007) Synaptotagmin I and II are present in distinct subsets of central synapses. J Comp Neurol 503:280–296.

Freed MA (2000) Parallel cone bipolar pathways to a ganglion cell use different rates and amplitudes of quantal excitation. J Neurosci 20:3956–3963.

Ghosh KK, Bujan S, Haverkamp S, Feigenspan A, Wässle H (2004) Types of bipolar cells in the mouse retina. J Comp Neurol 469:70–82.

Hashimoto K, Ichikawa R, Kitamura K, Watanabe M, Kano M (2009) Translocation of a "winner" climbing fiber to the Purkinje cell dendrite and subsequent elimination of "losers" from the soma in developing cerebellum. Neuron 63:106–118.

Haverkamp S, Grünert U, Wässle H (2000) The cone pedicle, a complex synapse in the retina. Neuron 27:85–95.

Haverkamp S, Wässle H, Duebel J, Kuner T, Augustine GJ, Feng G, Euler T (2005) The primordial, blue-cone color system of the mouse retina. J Neurosci 25:5438–5445.

Hopkins JM, Boycott BB (1996) The cone synapses of DB1 diffuse, DB6 diffuse and invaginating midget, bipolar cells of a primate retina. J Neurocytol 25:381–390.

Huang L, Max M, Margolskee RF, Su H, Masland RH, Euler T (2003) G protein subunit G gamma 13 is coexpressed with G alpha o, G beta 3, and G beta 4 in retinal ON bipolar cells. J Comp Neurol 455:1–10.

Huberman AD, Feller MB, Chapman B (2008) Mechanisms underlying development of visual maps and receptive fields. Annu Rev Neurosci 31:479–509.

Jefferis GS, Vyas RM, Berdnik D, Ramaekers A, Stocker RF, Tanaka NK, Ito K, Luo L (2004) Developmental origin of wiring specificity in the olfactory system of Drosophila. Development 131:117–130.

Keeley PW, Reese BE (2010) Role of afferents in the differentiation of bipolar cells in the mouse retina. J Neurosci 30:1677–1685.

Kerschensteiner D, Morgan JL, Parker ED, Lewis RM, Wong RO (2009) Neurotransmission selectively regulates synapse formation in parallel circuits in vivo. Nature 460:1016–1020.

Kim IJ, Zhang Y, Meister M, Sanes JR (2010) Laminar restriction of retinal ganglion cell dendrites and axons: subtype-specific developmental patterns revealed with transgenic markers. J Neurosci 30:1452–1462.

Klausberger T, Somogyi P (2008) Neuronal diversity and temporal dynamics: the unity of hippocampal circuit operations. Science 321:53–57.

Leamey CA, Van Wart A, Sur M (2009) Intrinsic patterning and experience-dependent mechanisms that generate eye-specific projections and binocular circuits in the visual pathway. Curr Opin Neurobiol 19:181–187.

Lee SC, Cowgill EJ, Al-Nabulsi A, Quinn EJ, Evans SM, Reese BE (2011) Homotypic regulation of neuronal morphology and connectivity in the mouse retina. J Neurosci 31:14126–14133.

Masland RH (2001) The fundamental plan of the retina. Nat Neurosci 4:877–886.

Millard SS, Flanagan JJ, Pappu KS, Wu W, Zipursky SL (2007) Dscam2 mediates axonal tiling in the Drosophila visual system. Nature 447:720–724.

Morgan JL, Dhingra A, Vardi N, Wong RO (2006) Axons and dendrites originate from neuroepithelial-like processes of retinal bipolar cells. Nat Neurosci 9:85–92.

Morgan JL, Soto F, Wong RO, Kerschensteiner D (2011) Development of cell type-specific connectivity patterns of converging excitatory axons in the retina. Neuron 71:1014–1021.

Morgans CW, Ren G, Akileswaran L (2006) Localization of nyctalopin in the mammalian retina. Eur J Neurosci 23:1163–1171.

Mumm JS, Williams PR, Godinho L, Koerber A, Pittman AJ, Roeser T, Chien CB, Baier H, Wong RO (2006) In vivo imaging reveals dendritic targeting of laminated afferents by zebrafish retinal ganglion cells. Neuron 52:609–621.

Nomura A, Shigemoto R, Nakamura Y, Okamoto N, Mizuno N, Nakanishi S (1994) Developmentally regulated postsynaptic localization of a metabotropic glutamate receptor in rat rod bipolar cells. Cell 77:361–369.

Niell CM (2006) Theoretical analysis of a synaptotropic dendrite growth mechanism. J Theor Biol 241:39–48.

Niell CM, Meyer MP, Smith SJ (2004) In vivo imaging of synapse formation on a growing dendritic arbor. Nat Neurosci 7:254–260.

Nikonov SS, Brown BM, Davis JA, Zuniga FI, Bragin A, Pugh EN Jr, Craft CM

(2008) Mouse cones require an arrestin for normal inactivation of phototransduction. Neuron 59:462–474.

Poché RA, Raven MA, Kwan KM, Furuta Y, Behringer RR, Reese BE (2008) Somal positioning and dendritic growth of horizontal cells are regulated by interactions with homotypic neighbors. Eur J Neurosci 27:1607–1614.

Reese BE, Raven MA, Stagg SB (2005) Afferents and homotypic neighbors regulate horizontal cell morphology, connectivity, and retinal coverage. J Neurosci 25:2167–2175.

Ren L, Liang H, Diao L, He S (2010) Changing dendritic field size of mouse retinal ganglion cells in early postnatal development. Dev Neurobiol 70:397–407.

Sanes JR, Yamagata M (2009) Many paths to synaptic specificity. Annu Rev Cell Dev Biol 25:161–195.

Tyzio R, Represa A, Jorquera I, Ben-Ari Y, Gozlan H, Aniksztejn L (1999) The establishment of GABAergic and glutamatergic synapses on CA1 pyramidal neurons is sequential and correlates with the development of the apical dendrite. J Neurosci 19:10372–10382.

Vardi N, Morigiwa K, Wang TL, Shi YJ, Sterling P (1998) Neurochemistry of the mammalian cone 'synaptic complex'. Vision Res 38:1359–1369.

Vaughn JE, Barber RP, Sims TJ (1988) Dendritic development and preferential growth into synaptogenic fields: A quantitative study of Golgi-impregnated spinal motor neurons. Synapse 2:69–78.

Waites CL, Craig AM, Garner CC (2005) Mechanisms of vertebrate synaptogenesis. Annu Rev Neurosci 28:251–274.

Wässle H (2004) Parallel processing in the mammalian retina. Nat Rev Neurosci 5:747–757.

Wässle H, Puller C, Müller F, Haverkamp S (2009) Cone contacts, mosaics, and territories of bipolar cells in the mouse retina. J Neurosci 29:106–117.

Williams ME, Wilke SA, Daggett A, Davis E, Otto S, Ravi D, Ripley B, Bushong EA, Ellisman MH, Klein G, Ghosh A (2011) Cadherin-9 regulates synapse-specific differentiation in the developing hippocampus. Neuron 71:640–655.

Wong GT, Ruiz-Avila L, Margolskee RF (1999) Directing gene expression to gustducin-positive taste receptor cells. J Neurosci 19:5802–5809.

Zhu H, Luo L (2004) Diverse functions of N-cadherin in dendritic and axonal terminal arborization of olfactory projection neurons. Neuron 42:63–75.

Zhu X, Ma B, Babu S, Murage J, Knox BE, Craft CM (2002) Mouse cone arrestin gene characterization: promoter targets expression to cone photoreceptors. FEBS Lett 524:116–122.

Zou DJ, Feinstein P, Rivers AL, Mathews GA, Kim A, Greer CA, Mombaerts P, Firestein S (2004) Postnatal refinement of peripheral olfactory projections. Science 304:1976–1979.